SYNTHESIS AND LUMINESCENCE PROPERTIES OF GREEN EMITTING TERBIUM DOPED ZINC PYROPHOSPHATE PHOSPHOR FOR UV-LED APPLICATIONS

[1]H. R. Shaikh, [2]Sayyed Asra, [3]Z. S. Khan
[1]Lecturer, [2]Research Student, [3]Assistant Professor
[1]Department of Physics,
[1]Government Polytechnic, Murtizapur, India.

Abstract: Terbium doped Zinc Pyrophosphate ($Zn_2P_2O_7$) is prepared first time by economical, simple and time saving slow vaporization synthesis technique keeping in mind its luminescence properties. XRD analysis and FTIR characteristics are carried out to confirm the structure and bonding of its constituents respectively. Surface morphology was studied by SEM images. The excitation spectra of $Zn_2P_2O_7$: Tb^{3+} consists of single narrow band peaking at about 236 nm, which can be ascribed to the f-d absorption transition of Tb^{3+} activators. The emission spectrum of $Zn_2P_2O_7$: Tb^{3+} consists of a series of sharp lines peaking at 489, 544, 586 and 622 nm corresponding to the $5D_4$-$7F_j$ (j=3, 4, 5, 6) inner-shell transition of the Tb^{3+} ions. Among the emission lines from the $5D_4$ state the dominant emission is observed at 544 nm, corresponding to the $5D_4$-$7F_5$ transition. The $5D_4$-$7F_5$ emission line is the strongest in nearly all host crystals when the Tb^{3+} concentration is a few mol % or higher because this transition has the largest probability for both electric-dipole and magnetic-dipole induced transitions. The intensity of 489 nm line, which corresponds to $5D_4$-$7F_6$ transition of Tb^{3+} ions is comparable and about one half the intensity of $5D_4$-$7F_5$ line. The intensity of the emission lines 586 and 622 nm is weak and corresponds to $5D_4$-$7F_4$ and $5D_4$-$7F_3$ transition of Tb^{3+} ions. Hence this phosphor may find applicable for UV-LED**.**

Index Terms **– Phosphate, Terbium; Photoluminescence, UV-LED.**

I. INTRODUCTION

Pyrophosphates with divalent metal ions are as well as alkaline earth metals are of great interest to the researchers. Apart from these, some are characterized by cation of small radii, have closely related structures in all their polymorphs [1] while others show four polymorphs [2-7]. Cadmium pyrophosphates are also investigated for various applications [8]. We tried a new method for the synthesis of pyrophosphates called slow Vaporization method keeping in mind the luminescence properties of it. We have already study rare earth doped phosphates $Ca_2P_2O_7$ by solution combustion synthesis method [9-13]. Not only doped but also pure pyrophosphates are supposed to be very important because of their multipurpose belongings including luminescent, dielectric, semiconductor, catalytic, magnetic, fluorescent and ion-exchange properties. Recently, Doat et al [14] as well as so many researchers [15-19] proposed the luminescent applications of europium-doped calcium pyrophosphates and hafnium pyrophosphate. Hence we proposed the luminescence properties of terbium doped Zinc Pyrophosphate $Zn_2P_2O_7$ phosphor for it's used in white LED applications.

.

II. EXPERIMENTAL

Polycrystalline $Zn_2P_2O_7$: Tb^{3+} phosphor is prepared by slow vaporization method [20]. Strontium nitrate [Zn $(NO_3)_2$] and di-amonium hydrogen orthophosphate [$(NH_4)_2HPO_4$] is added together with Tb_4O_7 (activator). Doubled distilled water is added in this combination. Mixing thoroughly about 10 minutes, milky solution is obtained. Now this solution is kept for slow evaporation at 100℃ for about 8 hours. The obtained white precipitate was kept under hot light for a complete night. The powder is then thoroughly mixed in the agate mortar. Now this powder is kept in previously heated furnace at 800 °C for 1 hour. The entire samples are now ready for characterizations.

The prepared sample was confirmed by Rigaku Miniflex X-Ray Diffractometer with scan speed of 2.00 deg/ min and with Cu Kα radiation (λ = 1.5406 Å). Scanning Electron Microscope (SEM) images of the sample are taken.

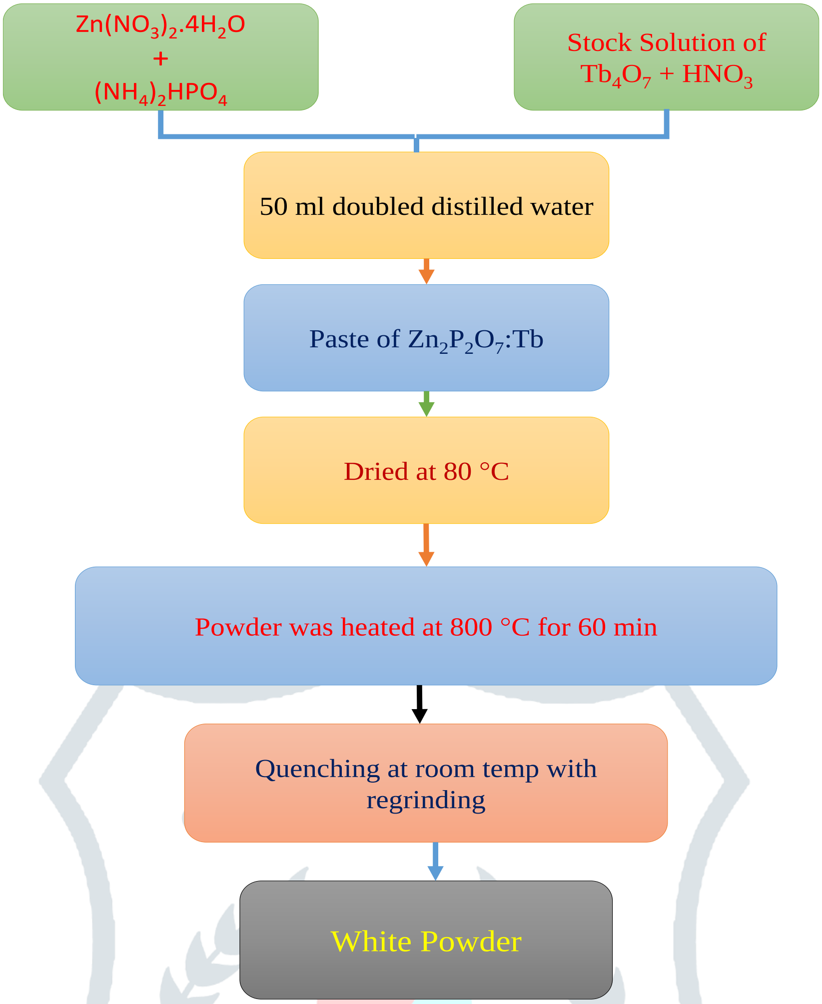

Figure 1. Flow Chart for the preparation of $Zn_2P_2O_7$: Tb

III. RESULTS AND DISCUSSION

3.1 XRD Analysis

The XRD patterns of $Zn_2P_2O_7$ with Tb as dopant is presented in Fig. 1. The XRD results indicate that all the patterns agree with the standard JCPDS file 08-0238, and dopant ions does not cause any significant change in the host structure. The α-$Zn_2P_2O_7$ phase has a monoclinic crystal system with C2/m space group. The cell parameters are 19.59 Å, 8.282 Å, 9.103 Å, β= 100.2, Z=12, and V = 1453.6 Å^3

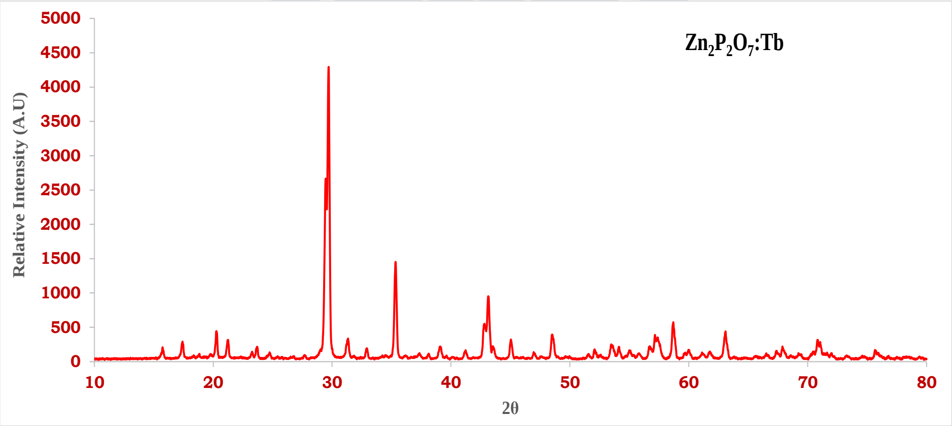

Figure 2. XRD of $Zn_2P_2O_7$: Tb.

Table 1: Crystallography date for $Zn_2P_2O_7$ lattice

Z	12
Crystal System	Monoclinic
Lattice	End Centered
Space Group	C2/m
Formula Weight	304.70
Density	4.24 g/cm^{-3}
Lattice Parameter	
a (A.U)	19.59
b (A.U)	8.282
c (A.U)	9.103
B	100.2°

3.2 Crystal Structure

As shown in Fig. 3, the $[P_2O_7]$ groups connect with each other by corner sharing to form a 3D network, and the Zn^{2+} ions locate at the polyhedral sites in the P–O network. [21]

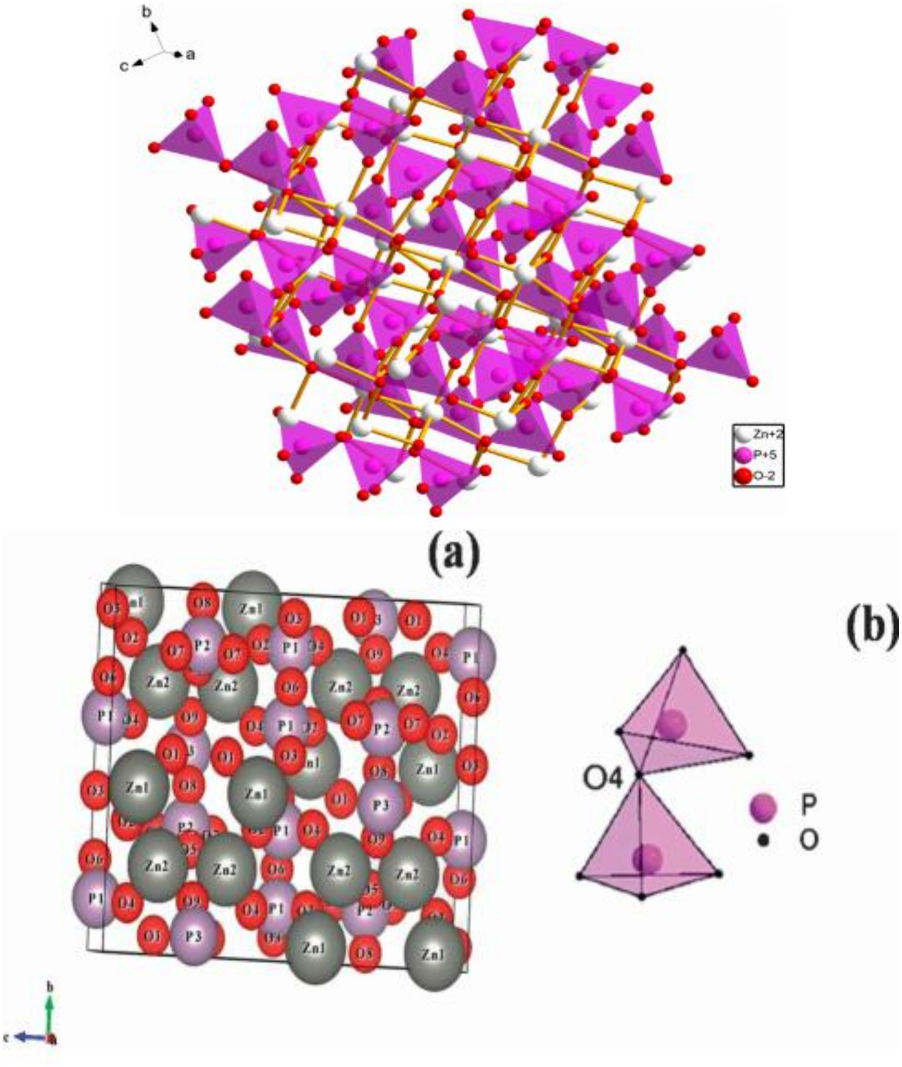

Figure 3. Schematic Crystal Structure of $Zn_2P_2O_7$

3.3 Morphology

SEM image is represented in Fig. 4 for $Zn_2P_2O_7$: Tb^{3+} material. The material shows irregular shape expanded particle structure. It shows the sizes of particles from 0.5 µm to 5 µm range.

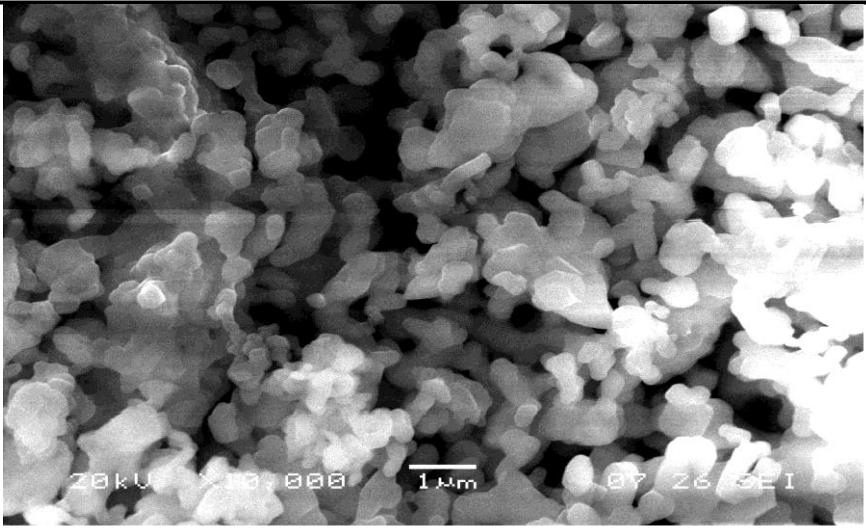

Figure 4. SEM image of $Zn_2P_2O_7$:Tb

3.4 FTIR Analysis

Fig. 5 represents the Fourier transformed infrared spectroscopy (FTIR) spectra for $Zn_2P_2O_7$:Tb Material. The FTIR revealed prominent absorption with peaks for $Zn_2P_2O_7$:Tb are at 3670 cm^{-1}, 2971 cm^{-1}, 1065 cm^{-1}, 1029 cm^{-1}, 1009 cm^{-1}, 949 cm^{-1}, 720 cm^{-1}, 607 cm^{-1} as shown in figure. The IR peak at about 1029 and 1065 cm^{-1} is for P-O asymmetric stretching bonds used for the preparation of $Zn_2P_2O_7$:Tb. The peaks at about 909 cm^{-1} and 990 cm^{-1} P-O symmetric stretching bonds. The IR absorption at wave numbers smaller than 500 cm^{-1} mainly originates from the lattice dynamic modes. A distinguished peak at 723.93 cm^{-1} is from the OH hydroxyapatite group is visible in spectrum. The absence of peaks in the range of 1550 - 2500 cm^{-1} supports the complete removal of residual nitrate and organic matter. The peaks at about 550 cm^{-1} is for O-P-O bonding. The IR spectrum confirms the existence of both trigonally and tetrahedrally coordinated boron atoms, consistent with the results obtained from the crystallographic study [22-24].

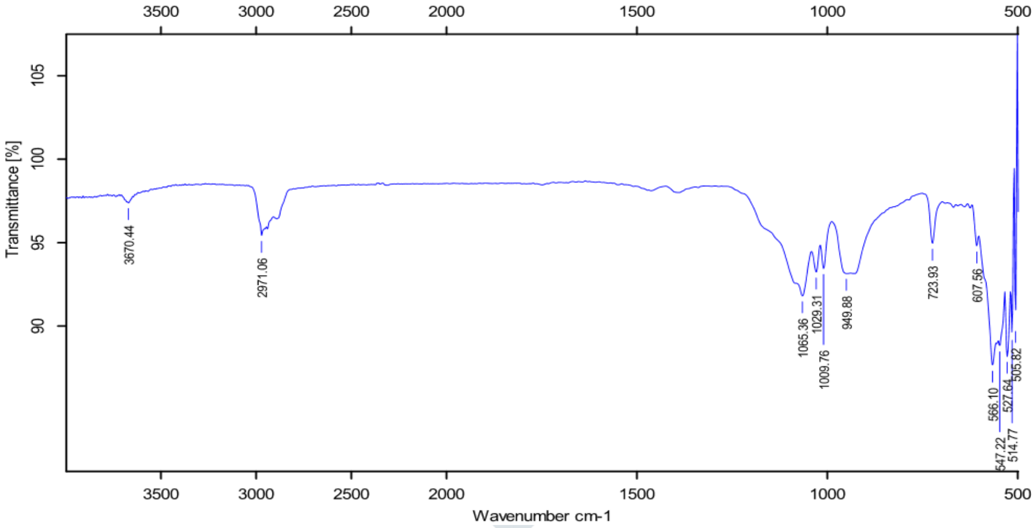

Figure 5. FTIR Analysis of $Zn_2P_2O_7$

3.5 Photoluminescence Studies

Figure 6 shows a partial energy level diagram of trivalent terbium with labeled transitions that correspond to the observed emission lines. The intensity of blue fluorescence from the $5D_3$ level is highly dependent on the terbium concentration. Since the energy difference between $5D_3$ and $5D_4$ levels is approximately equal to the energy difference between $7F_0$ and $7F_6$ levels, the excited electrons in the $5D_3$ level populate the $5D_4$ level through cross-relaxation, which involves a transfer of energy from an ion in the $5D_3$ state to a nearby ion in the ground state and can be represented as Tb^{3+} ($5D_3$) +Tb^{3+} (7Fj) → Tb^{3+} ($5D_4$) + Tb^{3+} ($7F_0$). At low Tb^{3+} concentration where cross-relaxation is improbable both blue 5D3-$7F_J$ and green $5D_4$-$7F_J$ emissions are observed, while the blue 5D3-7FJ (J= 1 to 6) emission is generally not observed in samples containing higher Tb^{3+} concentrations.

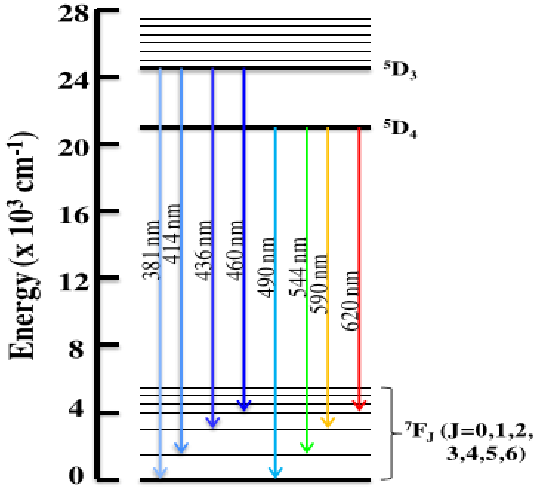

Fig 6: Energy Level diagram of Tb ion

Fig. 7 represents emission and excitation spectra of $Zn_2P_2O_7$: Tb^{3+}. The excitation spectra of $Zn_2P_2O_7$: Tb^{3+} consists of single narrow band peaking at about 236 nm, which can be ascribed to the f-d absorption transition of Tb^{3+} activators. The emission spectrum of $Zn_2P_2O_7$: Tb^{3+} consists of a series of sharp lines peaking at 489, 544, 586 and 622 nm corresponding to the $5D_4$-$7F_j$ (j=3, 4, 5, 6) inner-shell transition of the Tb^{3+} ions. Among the emission lines from the 5D4 state the dominant emission is observed at 544 nm, corresponding to the $5D_4$-$7F_5$ transition. The $5D_4$-$7F_5$ emission line is the strongest in nearly all host crystals when the Tb^{3+} concentration is a few mol % or higher because this transition has the largest probability for both electric-dipole and magnetic-dipole induced transitions. The intensity of 489 nm line, which corresponds to $5D_4$-$7F_6$ transition of Tb^{3+} ions is comparable and about one half the intensity of $5D_4$-$7F_5$ line. The intensity of the emission lines 586 and 622 nm is weak and corresponds to $5D_4$-$7F_4$ and $5D_4$-$7F_3$ transition of Tb^{3+} ions [25-27]

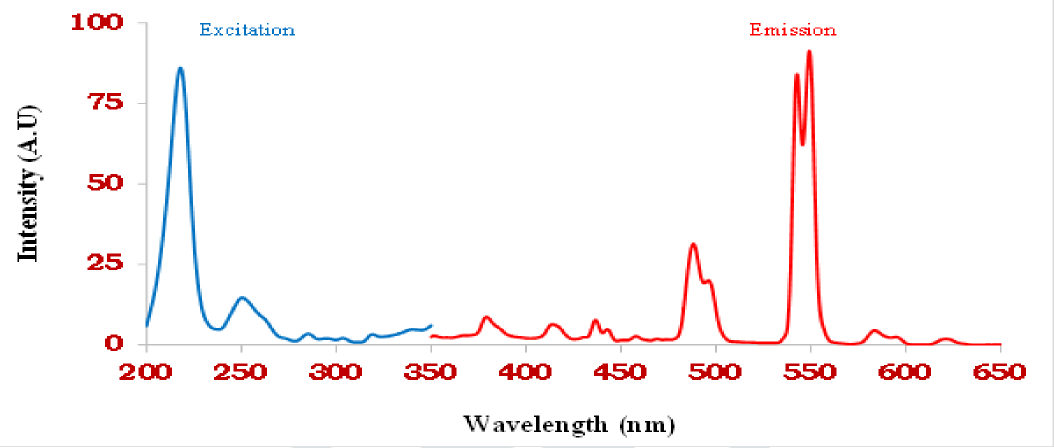

Figure 7. Excitation and Emission Spectra of $Zn_2P_2O_7$: Tb

3.6 CIE Chromatic Studies

The novel phosphors have excellent thermal stability and remarkable CIE chromaticity coordinate of (x = 0.2296, y = 0.7543), which points to its high potential as green emitting phosphor in lighting world [28]

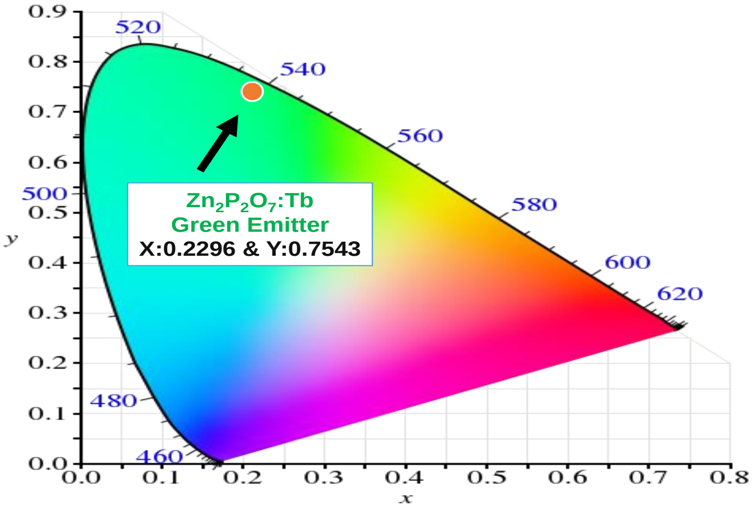

Figure 8. CIE diagram of $Zn_2P_2O_7$: Tb

4. Conclusions

In summary, a novel green phosphor $Zn_2P_2O_7$:Tb^{3+} was obtained via the slow vaporization method. The doped phosphor exhibits an intense green emission under the ultraviolet excitation. The novel phosphors have excellent thermal stability and remarkable CIE chromaticity coordinate of (x = 0.2296, y = 0.7543), which points to its high potential as green emitting phosphor in lighting world. The combination of Red, Green and Blue gives us White light.

III. ACKNOWLEDGMENT

The author is very much thankful to head, department of Physics and Electronics, GVISH, Amravati, for providing necessary research facilities.

REFERENCES

[1] K. Lukaszewicz, Bull. Acad.Po1. Sci. Ser. Sci. Chim, 15 (1967) 47-51.
[2] C. Calvo, Inorg. Chem. 7 (1968) 1345-1349.
[3] N. C. Webb, Acta Cryst, 21 (1966) 942-944.
[4] L. Hagman, I. Jansson, C. Magneli, Acta Chem. Scand., 22 (1968) 1419-1423.
[5] Z. S. Khan, N. B. Ingale, S. K. Omanwar, Mater. Lett., 158 (2015) 143-146.
[6] Z. S. Khan, N. B. Ingale, S. K. Omanwar, Materials Today: Proceedings 2 (2015) 4384-4389.
[7] Z. S. Khan, N. B. Ingale, S. K. Omanwar, AIP Conference Proceedings 1953 (2018) 070024
[8] P. K. L. Au, C. Calvo., Can. J. Chem. 45 (1967) 2297-2299.
[9] Z. S. Khan, N. B. Ingale, S. K. Omanwar, Environ Sci. Pollut. Res, 23 (2016) 9295-9302.
[10] Z. S. Khan, N. B. Ingale, S. K. Omanwar, Opt-Int J Light Electron Opt., 127 (2016) 9679-9682
[11] Z. S. Khan, N. B. Ingale, S. K. Omanwar, Opt-Int J Light Electron Opt., 127 (2016) 6062-6065
[12] K. Zamir, Z. S. Khan, N. B. Ingale, S. K. Omanwar, AIP Conference Proceedings 2104 (1), 030035
[13] D. N. Game, S. T. Taide, Z. S. Khan, N. B. Ingale, S. K. Omanwar, AIP Conference Proceedings 1728 (1), 020488
[14] A. Doat, F.Pelle, A. Lebugle, J. Solid State Chem. 178 (2005) 2354-2358.
[15] H. Assaaoudi, I. S. Butler, J. Kozinski, F. Belanger-Gariepy, J Chem Crystallogr 35 (2005) 809-812.
[16] T. Varga, A. P. Wilinson, M. S. Haluska, E. A. Payzant, J Solid State Chem 178 (2005) 3541-3544.
[17] I. C. Marcu, J. M. M. Millet, J. M. Herrmann, Catal Lett 78(2002) 273-276.
[18] C. H. Srilakshmi, K. Ramesh, P. Nagaraju, N. Lingaiah, P. S. S. Prasad, Catal Lett 106 (2006) 115-118.
[19] K. Fukuda, A. Moriyama, S. Hashimoto, J Solid State Chem 177 (2004) 3514-3516.
[20] M. Rathod, Z. S. Khan, N. B. Ingale, S. K. Omanwar, J of Emerging Tech and Innovative Res., 6 (2019), 460-463.
[21] S. K. Gupta, M. Mohapatra, S. V. Godbole, V. Natarajan, RSC Adv., 3 (2013) 20046-20053.
[22] N. Khay, A. A. Ennaciri, M. Harcharras, Vib Spectrosc., 27 (2001) 119-123.
[23] N. Khay, A. A. Ennaciri, J Alloys Compd 323 (2001) 800-803.
[24] M. S. Idrissi, L. Rghioui, R. Nejjar, L. Benarafa, M. S. Idrissi, A. Lorriaux, F. Wallart, Spectrochim Acta Part A 60 (2004) 2043-2045.
[25] R. P. Rao, J. Electrochem. Soc., 150 (2003) H165
[26] Z. S. Khan, N. B. Ingale, S. K. Omanwar, International Journal of Luminescence and its Applications 5 (4), 471-474
[27] Z. S. Khan, N. B. Ingale, S. K. Omanwar, Advanced Science Letters 22 (2015) 164-166
[28] Z. S. Khan, N. B. Ingale, S. K. Omanwar, Journal of Advances in Applied Sciences and Technology 1 (2014) 277-279